Voltammetry and Molecular Assembly of G-quadruplex DNAzyme on Single-crystal Au(111)-electrode Surfaces – Hemin as an Electrochemical Intercalator

Zhang, Ling; Ulstrup, Jens; Zhang, Jingdong

Published in:
Faraday Discussions

Link to article, DOI:
10.1039/C6FD00091F

Publication date:
2016

Document Version
Peer reviewed version

View Article Online
DOI: 10.1039/C6FD00091F

Voltammetry and Molecular Assembly of G-quadruplex DNAzyme on Single-crystal Au(111)-electrode Surfaces – Hemin as an Electrochemical Intercalator

Ling Zhang, Jens Ulstrup and Jingdong Zhang**

Department of Chemistry, Technical University of Denmark, Building 207, Kemitorvet, DK-2800 Kgs. Lyngby, Denmark. Email, jz@kemi.dtu.dk, ju@kemi.dtu.dk.

Abstract

DNA quadruplexes (qs's) are a class of "non-canonical" oligonucleotides (OGNs) composed of stacked guanine (G) quartets stabilized by specific cations. Metal porphyrins selectively bind to G-qs complexes to form what is known as DNAzyme, which can exhibit peroxidase and other catalytic activity similar to heme group metalloenzymes. In the present study we investigate the electrochemical properties and the structure of DNAzyme monolayers on single-crystal Au(111)-electrode surfaces using cyclic voltammetry and scanning tunnelling microscopy under electrochemical potential control (*in situ* STM). The target DNZyme is formed from a single-strand OGN with 12 guanines and iron (III) porphyrin IX (hemin), and assembles on Au(111) by a mercapto alkyl linker. The DNAzyme monolayers exhibit a strong pair of redox peaks at 0.0 V (NHE) at pH 7 in acetate buffer, shifted positively by about 50 mV compared to free hemin weakly physisorbed on the Au(111)-electrode surface. The voltammetric hemin signal of DNZyme is enhanced 15 times compared with that of hemin adsorbed directly on the Au(111)-electrode surface. This is indicative both that a close to dense DNAzyme monolayer is formed and that hemin is strongly bound to the immobilized 12G-qs in well-defined orientation favorable for interfacial ET with a rate constant of 6.0 ± 0.4 s^{-1}. This is supported by *in situ* STM which discloses single-molecule G-quartet structures with a size of 1.6 ± 0.2 nm.

1. Introduction

DNA-based single- and double-strand (ss and ds) oligonucleotides (OGNs) immobilized on

View Article Online
DOI: 10.1039/C6FD00091F

solid surfaces are focus systems in molecular diagnostics and other chemical and biological sensing[1-4]. Long-range electron transfer (ET) mechanisms in redox metalloprotein systems have become understood in increasing detail over the last couple of decades[5-8]. The more recent discovery of long-range photo-induced ET in ds OGNs has triggered strong interest in the fundamental mechanisms of DNA-based electron and hole conductivity[9-16]. Electron or hole "hopping", with full vibrational relaxation between each single-charge hop has emerged as an attractive mechanism for photo-induced OGN electronic conductivity. This notion is, however, faced with challenges in interfacial electrochemical ET in redox marked surface immobilized OGN molecules[11-13,17-20]. Much lower energies than in photochemical ET are involved here, questioning the feasibility of actual electron or hole generation (reduction and oxidation) in the nucleobase pairs in the electrochemical potential ranges accessible. It was also found that in addition to the Faradaic ET processes between the electrode surface and intercalated redox probes[12,13,17-20], potential induced surface structural changes in the OGN adlayer on atomically planar Au(111)-electrode surfaces can induce capacitive voltammetric signals in the presence of multiply charged counter ions (spermidine)[20] that stabilize the ds form[21,22]. These peaks can resemble the Faradic signals of the ET probes in redox marked OGNs otherwise forwarded as fingerprints of long-range electrochemical ET along the axis of the ds OGNs[11,12,17-19]. Central issues regarding the mechanisms of interfacial electrochemical ET of redox probes intercalated or covalently bound to immobilized target OGNs are therefore open.

We report here a study of electrochemical OGN conductivity using a different approach with the following perspectives:

- Our molecular target is a "non-canonical" OGN form, viz. a guanine-rich OGN quadruplex (G-qs) instead of the ds OGN. G-qs structures can be viewed as stacking of a variable number of G-quartets folding along ss guanine-rich strands[23-26]. G-qs's form spontaneously in aqueous biological buffers in the presence of specific cations, potassium or sodium ions in particular, Figure 1A[26]. The G-qs's resemble the telomer ends in the chromosomes[23-28]. Their natural biological functions are largely unknown, but G-qs peptide binding and recognition has attracted interest in peptide sensing, therapy and other biotechnology[26-28].
- The rigid G-qs structure compared with ds OGNs offers a perspective for facile long-range ET as reflected in good conductivity of G-qs's[29-32]. As for spermidine induced ds OGN

View Article Online
DOI: 10.1039/C6FD00091F

structural tightening, G-qs's might also show capacitive voltammetry that reflects reorientation of the rigid G-qs structure at the well-defined Au(111)-electrode surfaces.

- Studies of the electrochemical behavior of G-qs's immobilized on polycrystalline Au-electrode surfaces have been reported[33,34]. These have, for example been brought to distinguish between ds and qs's structures based on surface accessibility of small mobile redox molecules such as $[Ru(NH_3)_6]^{2+/3+}$ and $[Fe(CN)_6]^{4-/3-}$. In the present report, we use instead firstly atomically planar single-crystal Au(111)-electrodes onto which the target G-qs's are linked via a protected thiol linker and a chain of six methylene groups. Use of this configuration enables, secondly structural mapping of the immobilized G-qs molecules by electrochemical scanning tunnelling microscopy (*in situ* STM) to single-molecule resolution.
- Finally, recent reports have pointed to the feasibility of both structural and functional single-molecule mapping of complex molecules including both redox metalloproteins and redox marked DNA-based molecules, by scanning tunnelling current/overpotential spectroscopy under electrochemical potential control (*in situ* STS)[34,35]. These studies include the use of a redox probe intercalated or covalently bound to the OGN frame and electron exchange between the redox probe and the electrode.[36-39]. Other recent studies have addressed single-molecule conductivity *in situ* using direct conductivity approaches[39]. The G-qs structure can be combined with iron (III) porphyrin IX (hemin) through л–л stacking between the porphyrin and the guanine quartet plane[26,40,41]. This "hybrid", known as DNAzyme catalyzes the reduction of dioxygen or hydrogen peroxide similarly to the peroxidase enzyme class. The hemin molecule is believed to be terminally bound to either of the two terminal quartet planes of the G-qs, Figure 1A and 1B. In the present work hemin is thus a redox probe that could potentially monitor long-range electrochemical ET through the G-qs molecules.

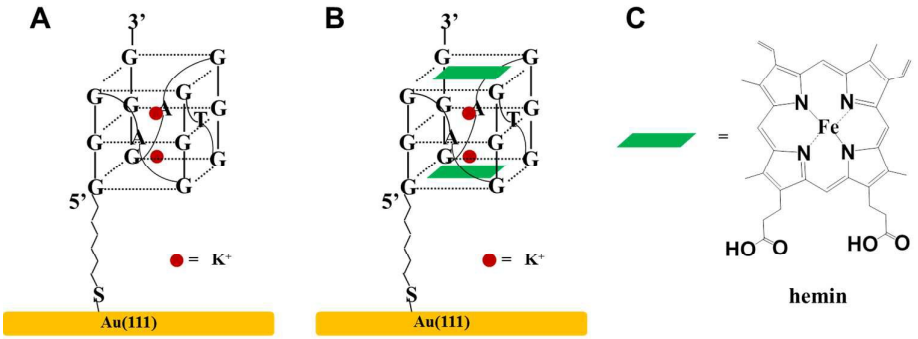

Figure 1. (A) Scheme of G-qs structure stabilized by K^+ ions. (B) Scheme of G-qs DNAzyme with

View Article Online
DOI: 10.1039/C6FD00091F

terminally bound hemin molecules. (C) Molecular structure of hemin.

We address first as a reference structural and electrochemical properties of hemin adsorbed on bare Au(111)-electrode surfaces using a combination of cyclic voltammetry and *in situ* STM to single-molecule resolution. This is fraught with some challenge as hemin is adsorbed much more weakly on Au(111)-electrode surfaces in biologically pH-ranges than on, say highly oriented pyrolytic graphite (HOPG) surfaces. We explore next the interfacial electrochemical structure and dynamics of the shortest, ss 15-base OGN, 5'-SH-$(CH_2)_6$-GGG A GGG T GGG A GGG (MW 5147.3, T30695)[26], folded into the G-qs structures in the presence of potassium ions, and attached to the Au(111)-electrode surface via a protected –S-$(CH_2)_6$- linker. The 12G target is addressed both in pure form and with terminally bound hemin, using the same combination of CV and *in situ* STM as for hemin itself. Notable differences between the adlayers of pure and hemin marked G-qs (DNAzyme) are observed. Intriguingly, both the electrochemical hemin signal and the UV-vis absorption spectra of the G-qs DNAzyme in the hemin Soret band region are much stronger than for hemin itself, indicative that a robust organized and dense 12G-qs/hemin adlayer has formed.

Based on *in situ* STM, it is shown that the single 12G-qs molecular entities can organize collectively into monolayers on the Au(111)-electrode surface possibly via hydrogen bond interactions among the guanine quartets. The domains are composed of alternating quartets and octagons with intermolecular distance of about 1.6 ± 0.2 nm. The organization follows, intriguingly adsorption patterns of single-G-quartets of guanine molecules on Au(111)-surfaces at 350 K in ultra-high vacuum (UHV)[42]. Approaches such as these to G-qs/hemin monolayers have not been reported before.

2. Experimental

2.1 Chemicals and Preparations

Chloroprotoporphyrin IX iron (III) (hemin, porcine, $C_{34}H_{32}ClFeN_4O_4$, ≥ 98.0%), sodium hydroxide (NaOH, 99.99%), sodium acetate (CH_3COONa, 99+%), potassium acetate (CH_3COOK, for molecular biology, ≥ 99.0%), were all from Sigma-Aldrich and used without further purification. Hemin solution was prepared by dissolving 1 mM hemin in 10 mM sodium hydroxide and diluting to 2.5 μM with sodium acetate buffer at pH 7. Millipore water (Milli-Q, 18.2 MΩ cm) was used throughout. The purified 12G oligonucleotide (5'-SH-

View Article Online
DOI: 10.1039/C6FD00091F

$(CH_2)_6$-GGG A GGG T GGG A GGG, MW 5147.3) was synthesized using commercially available building blocks at the Nucleic Acid Center, University of Southern Denmark.

The 12G samples were prepared in 0.51 μM stock solution in 5 mM sodium acetate solution at pH 7.2 and stored at − 20°C. Before use, the solution was annealed at 88 °C for 10 min to ensure complete melting and then cooled slowly to room temperature[26,40].

2.2 Preparation of G-Quadruplex DNAzyme Monolayers on Au(111) Electrode Surfaces

Single-crystal Au(111) bead electrodes (ca. ø 3 mm) were prepared as described and checked by cyclic voltammetry in 0.1 M H_2SO_4[43-47]. The Au(111) bead electrodes were cleaned prior to use by H_2 flame annealing and quenched in Millipore water saturated with H_2.

To form the G-qs quadruplex structures, 0.51 μM 12G stock solution was mixed with 10 μM potassium acetate at room temperature (21°C). After 45 min, the G-qs formed was incubated with 0.25 μM hemin solution for one hour leading to binding or intercalation of hemin molecules in 12G-qs G-qs/hemin complexes, here denoted as DNAzyme. After quenching in Millipore water, the Au(111)-electrodes were soaked in DNAzyme solution for 1 hour, rinsed with a mixture of 5 mM sodium and 10 μM potassium acetate, and then used in the cyclic voltammetry and *in situ* STM.

2.3 Preparation of Hemin Monolayers on Au(111)- Electrode Surfaces

Self-assembled monolayers of hemin molecules were prepared by immersing the freshly cleaned single-crystal Au(111)-electrodes in 0.25 μM or higher hemin solutions in 5 mM sodium acetate buffer, pH 7.2 for 1 hour. The modified electrodes were gently rinsed and kept in the same buffer for further use.

2.4 Instrumentation

The Au(111)-electrodes for cyclic voltammetry were used in the hanging meniscus mode. Cyclic voltammetry was performed using an Autolab potentiostat/galvanostat system (Eco Chemie, The Netherlands) controlled by the NOVA 2.0 software. An electrochemical setup including a cell and three-electrode configuration was employed as described[43-47]. A bright platinum wire was used as counter electrode and a freshly prepared reversible hydrogen electrode (RHE) exposed to the same supporting electrolyte and bubbled with pure H_2 as the

View Article Online
DOI: 10.1039/C6FD00091F

reference electrode. The RHE was calibrated against the saturated calomel electrode (SCE) after each experiment. The electrolyte was deoxygenated by bubbling purified argon (Chrompack, 5 N) into the solution for one hour, and an argon atmosphere maintained throughout the experiments. UV-visible absorbance spectra were recorded using an Agilent G1103A Spectrophotometer.

A Pico SPM instrument (Molecular Imaging Co., U.S.A) was used for *in situ* STM. Home-made STM Tips were prepared by etching either tungsten or Pt/Ir (80/20) wire and coated with Apiezon wax[47]. The *in situ* STM cell was an in-house-built three-electrode PTFE cell with two Pt wires as reference and counter electrodes. The Au(111)-electrode was the substrate. The potential of the Au(111)-electrode substrate and of the tungsten or Pt/Ir tips was controlled in the supporting electrolyte by a bipotentiostat.

3. Results

3.1 Voltammetry of Hemin Monolayers on Au(111)-electrode surfaces

Hemin adsorbed on the Au(111)-electrode surface was found to display a complex behavior that reflects both protonation equilibria and dimer/oligomer formation on the surfaces in different pH-ranges. We shall communicate these observations elsewhere. Presently we focus on hemin surface behavior on a bare Au(111)-electrode surface in the same aqueous buffer, pH ≈ 7 as the stability range of surface immobilized G-qs to be probed by bound hemin.

Without the hemin monolayer, acetate adsorbs on the Au(111)-electrode surface, giving a set of strong and composite adsorption/desorption peaks in the range 0.1~0.6 V (vs. NHE), Figure 2A[44]. Hemin adsorption causes the acetate adsorption peaks largely to disappear, and a pair of peaks with a midpoint potential around – 0.05 V (NHE) appears instead, Figure 2B. This peak is fraught with a high capacitive background but conspicuous enough that the dependence of the peak height, i_p on the scan rate v could be determined. The i_p/v correlation is clearly linear up to about 0.5 V s^{-1}, Figure 2C, identifying the voltammetric behavior as surface confined.

The coverage of the hemin on the surface depends on the hemin concentration in the soaking solution. Taking the process to be a one-ET transition, the surface coverage was found to be about $(6.0 \pm 1.4) \times 10^{-13}$ mol · cm^{-2} from the peak area when the hemin adlayer was prepared from 0.25 μM hemin solution. If the adlayer is prepared from 0.5 μM hemin solution,

View Article Online
DOI: 10.1039/C6FD00091F

significantly stronger peak currents appear, Figure 2D, giving now a coverage of hemin molecules of (5.4 ± 0.4) × 10^{-12} mol · cm^{-2}. Assuming a dense monolayer of a 1 × 1 nm^2 molecular hemin entity, the coverage is 1.7 × 10^{-10} mol · cm^{-2}. If all the hemin molecules in 1 mL solution are adsorbed on a Au(111)-electrode with a diameter of 3.0 mm and form a monolayer, this would correspond to a hemin concentration of 0.012 μM. As hemin molecules are involved in an adsorption equilibrium between the electrode and solution, a concentration of 0.25 ~ 0.5 μM hemin appears insufficient to form a full monolayer on Au(111) surface.

The anodic and cathodic peak separation increases from about 60 mV at the lowest scan rates to about 113 mV at higher scan rates approaching 1 V s^{-1}, Figure 2D. At still higher scan rates the hemin monolayer seemed to loosen from the surface and the peak current dependence on the scan rate was replaced by a $i_p/v^{½}$ dependence (data not shown). The peak separation dependence on the scan rate up to 1 V s^{-1} enabled estimating the standard interfacial electrochemical ET rate constant, k_s using Laviron's method, giving the value of k_s ≈ 15 ± 2 s^{-1}. This value can be compared with the value found from hemin stacked onto G-qs, see Section 3.3.

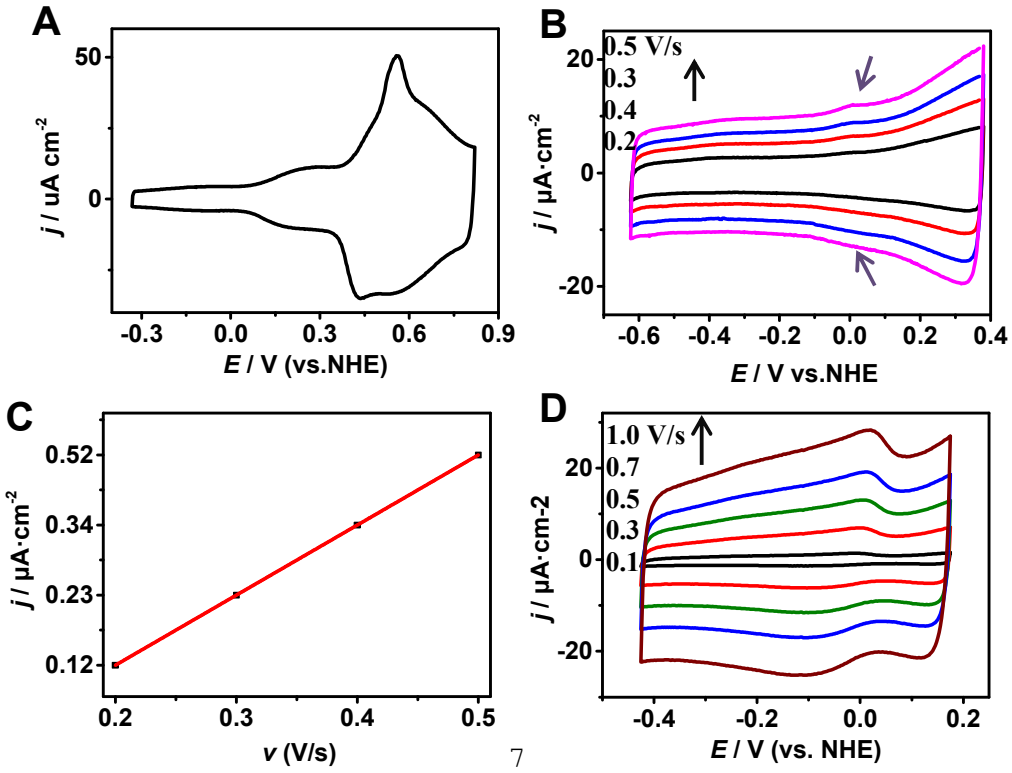

View Article Online
DOI: 10.1039/C6FD00091F

Figure 2. (A) Cyclic voltammetry (CV) of Au(111)-electrode in 5mM sodium acetate solution, pH 7.3. Scan rate, 0.2 V s^{-1}. (B) CV of hemin modified Au(111)-electrode at different scan rates. 5 mM sodium acetate, pH 7.1. The hemin adlayer prepared from 0.25 μM hemin solution, 5 mM sodium acetate, pH ~ 7. The arrows inserted at ≈ 0.0 V point to the (small) hemin Faradaic peaks. (C) Anodic peak current versus the scan rate. (D) CV of hemin modified Au(111)-electrode prepared from 0.5 μM hemin solution at different scan rates.

3.2 In Situ STM of Hemin Monolayers on Au(111)-Electrode Surfaces

In situ STM of the adlayer structure of hemin on the Au(111)-electrode surface in sodium hydroxide solution was recorded next. A full self-assembled monolayer (SAM) of hemin molecules was obtained by soaking the Au(111) electrode in 10 μM hemin aqueous solution at pH 12. This coverage is much higher than the coverage obtained by soaking in 0.25 μM hemin solution around pH 7. As shown in Figure 3A, ordered lines with 120° angle and 6.4 nm spacing on the atomically flat terrace were observed. These lines are attributed to the characteristic Au(111) herringbone ($\sqrt{\mathbf{3}} \times 22$) reconstruction lines on Au(111) and indicates clearly that the hemin molecules are physisorbed on the Au(111) surface.

Ordered arrays of hemin molecules are thus assembled on the reconstructed Au(111) surface. A close-up image is shown in Figure 3B. Detailed distance and angle analysis shows that one row of the adlayers is parallel to one of the atomic rows of the Au(111)-surface with a periodic distance of 1.2 ± 0.1 nm. The other row is perpendicular to the atomic row of the substrate underneath with the periodic distance 1.6 ± 0.2 nm. The surface structure is therefore assigned to a $c(4 \times 3\sqrt{\mathbf{3}})-2$ unit cell containing two hemin molecules. The unit cell is marked in Figure 3B and a likely surface binding mode is proposed in Figure 3C. The hemin plane is parallel to the Au(111)-surface probably supported by the –OH axial ligand adsorbed on the surface. Both hydrophobic and hydrophilic interactions act among the hemin molecules in the monolayer. The hemin molecule at the center is moreover mirror symmetric relative to the molecules at the corners of the rectangle, and the pairs stabilized by both hydrogen bonds and hydrophobic interactions between the hemin side groups[48-51]. The unit cell is close to the $c(5 \times 6\sqrt{\mathbf{3}})-2$ unit cell for Co(II)phthalocyanine on Au(111) reported by

View Article Online
DOI: 10.1039/C6FD00091F

Itaya and associates[52] but differs from the unit cells of octaethylporphyrin iron(III) chloride ($a \times b$ = 1.23 nm × 1.4 nm with an angle of 66°) on Au(111)[53] and hemin (1.22 nm × 1.34 nm with 68°) on HOPG[48]**.** These differences are most likely caused by different lateral interactions among the molecules and between the molecules and the electrode substrates[51]. Very different packing lattices in cysteine monolayers on Au(111)- and Au(110)-electrode surfaces in solution and vacuum have also been found[47,54].

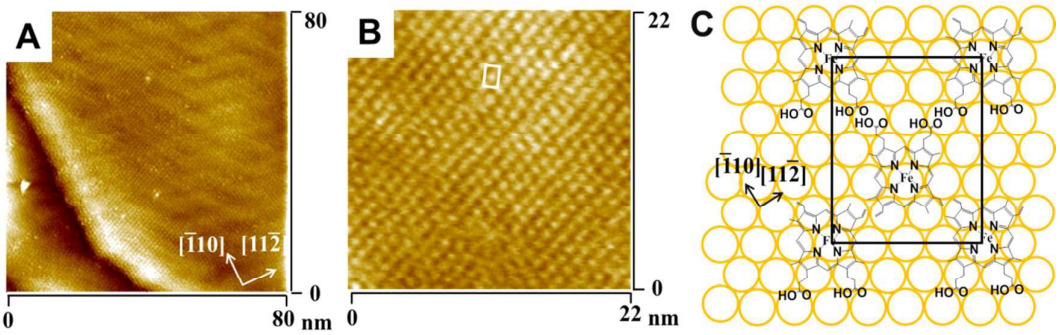

Figure 3. (A) and (B) *In situ* STM images of hemin monolayer on single-crystal Au(111)-electrode in 10 mM sodium hydroxide, pH 12. The electrode modified in 10 µM hemin in 10 mM sodium hydroxide solution. Working electrode potential E_{work} = 0.2 V (vs. NHE), tunnelling current I_{tunnel} = 0.04 nA. Bias voltage, V_{bias} = 0.26 V (A), V_{bias} = − 0.14 V (B). (C) Proposed model for iron porphyrin monolayer formed on Au(111) surface superimposed with a $c(4 \times 3\sqrt{\mathbf{3}})$-2 unit cell.

3.3 Cyclic Voltammetry of 12G-qs and DNAzyme SAMs

Our qs target, 12G-qs is the smallest G-qs with only three G-quartets. The DNAzyme is formed when hemin molecules are bound onto the 12G-qs ends by π-π interaction or intercalated into the 12G-qs structures. As shown in Figure 4A, the Soret absorption peak at 404 nm from the constructed DNAzyme is 20 times higher than the peak for the same concentration of free hemin in solution and furthermore red-shifted by 2 nm compared to that of free hemin molecules. Both spectral observations indicate that there is strong electronic interaction between hemin and the terminal quartet(s) in spite of the non-covalent nature of this interaction. The OGN absorption peak at 254 nm is maintained after binding of hemin.

The DNAzyme was investigated by cyclic voltammetry (CV). Hemin free 12G-qs or the DNAzyme complex was adsorbed on the Au(111)-electrode surface through the protected

View Article Online
DOI: 10.1039/C6FD00091F

SH-group. Figure 4B and C show CVs of hemin-free 12G-qs and the 12G-qs/hemin complex (DNAzyme), respectively. The CVs of hemin free 12G-qs show a broad featureless capacitive background in the potential range − 0.4 V to + 0.1 V. There is, however, also a conspicuous pair of peaks at ≈ − 0.4 V for the anodic peak and ≈ − 0.55 V for the cathodic peak (midpoint potential − 0.48 V). Indications of less well-defined peaks around + 0.2 V are not likely to be associated with hemin but either with adsorption of acetate or reconstruction lift of the Au(111)-electrode surface. The origin of the − 0.4 and − 0.55 V peaks is not clear. Reductive and oxidative desorption/re-adsorption cannot be excluded, but both the midpoint potential and shape of this low-potential pair resemble those for the capacitive peaks observed for 20-base pair ds ONS when the triply charged counter ion spermidine was present[20]. Spermidine is known to stabilize the ds form[21,22], and the peak –specific to base pair matching - was assigned to potential induced surface structural reorganization in the double-strand DNA adlayer which was further tentatively supported by *in situ* STM in the peak potential range. The –0.4/–0.55 V 12G-qs pair could have a similar origin, i.e. arise from surface reorientation or order/disorder transition in the SAM of the compact 12G-qs molecules. *In situ* STM imaging studies to explore the surface dynamics further are in progress.

Figure 4C shows CVs of the DNAzyme, i.e. hemin bound in the 12G-qs/hemin complex. In order to avoid having free hemin in the solution the complex was always prepared from a 2:1 G-qs/hemin mole ratio, leaving statistically one bound hemin molecule per 12G-qs/hemin complex. The most striking observation now is a strong signal at 0.0 V (vs. NHE), shifted positively by about 50 mV compared to the midpoint potential of hemin physisorbed on the Au(111)-electrode surface. This is strongly indicative of favorable interfacial ET of hemin bound to 12G-qs, possibly through the G-quadruplex structures, and further of high 12G-qs coverage on the Au(111)-electrode surface. The peak current of the strongly 12G-qs bound hemin is thus increased about 15 times compared to the physisorbed hemin on the Au(111)-electrode surface. The total amount of hemin bound to surface immobilized 12G-qs after π−π binding or intercalation is $(2.5 \pm 0.4) \times 10^{-11}$ mol · cm^{-2}, which is 40 times the amount of physisorbed hemin in Figure 2B. Both anodic and cathodic peak currents depend linearly on the scan rates, corresponding to surface behavior of the DNAzyme monolayer, Figure 5D. The anodic peak widths are in the 103~135 mV range at scan rates from 0.1 to 1.0 V/s. This

View Article Online
DOI: 10.1039/C6FD00091F

can be compared with the theoretical value (91 mV) for reversible one-electron transfer and supports that as an average, there is one bound hemin molecule per 12G-qs structural entity. The amount of the DNAzyme obtained from the CVs, $(2.5 \pm 0.4) \times 10^{-11}$ mol · cm^{-2} is not much lower than for a dense monolayer of 12G-qs/hemin, which is $(6.6 \pm 0.7) \times 10^{-11}$ mol · cm^{-2} obtained from the STM results, Section 3.4. The standard interfacial electron transfer rate constant k_s is 6.0 ± 0.4 s^{-1}, which is comparable even to that of the hemin monolayer itself adsorbed directly on the Au(111)-electrode surface (15 ± 2 s^{-1}, Section 3.1).

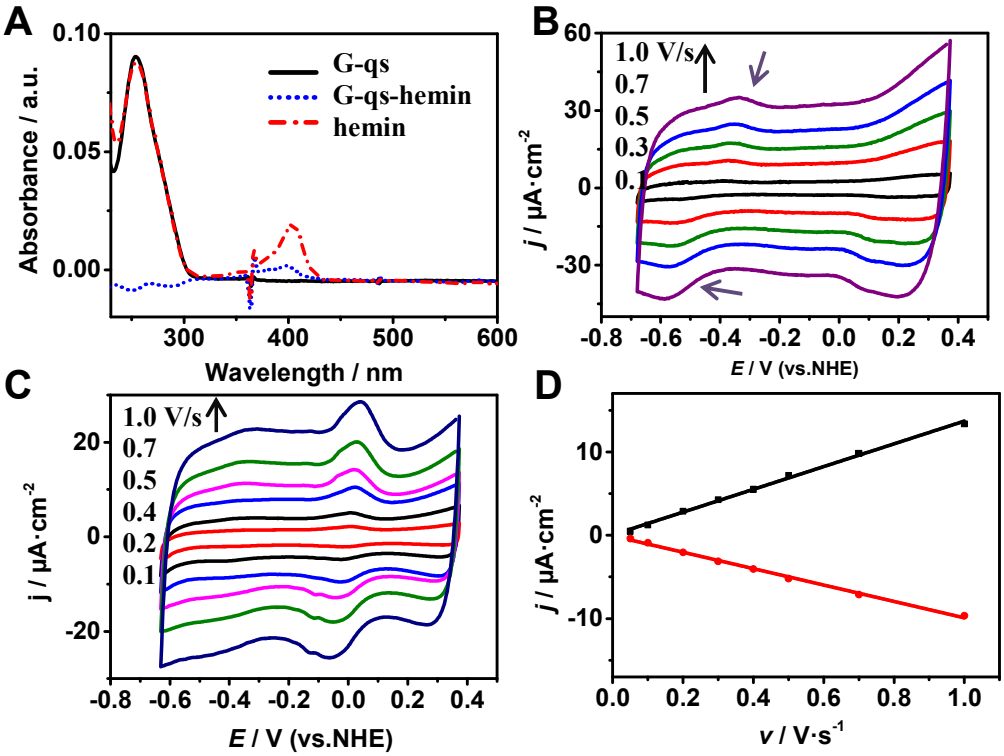

Figure 4. (A) UV-vis spectra of 0.5 μM 12G-qs, 0.5 μM 12G-qs with 0.25 μM hemin, and of 0.25 μM hemin solutions in 5 mM sodium acetate buffer with 10 μM K^+ ions at pH 7. (B) CVs of 12G-qs modified Au(111)-electrode in 5 mM sodium acetate, pH 7.2 at different scan rates. Tilted arrows show the voltammetric peaks discussed in the text. (C) CVs of DNAzyme modified Au(111)-electrode in 5 mM sodium acetate, pH 7.2 at different scan rates. (D) Anodic and cathodic peak currents versus scan rates.

3.4 In Situ STM of 12G-qs DNAzyme SAMs on Au(111)-surfaces

The DNAzyme adlayer assembled on the Au(111)-electrode surface was further characterized

View Article Online
DOI: 10.1039/C6FD00091F

by *in situ* STM, Figure 5. These data are somewhat preliminary, and further work is in progress. The potential applied to the sample is 0.49 V, which is the open circuit potential and the hemin redox center bound to 12G-qs is in the oxidized form Fe (III). Our present objective is thus to achieve single-molecule imaging, but tunnelling current/overpotential and bias voltage spectroscopy will be addressed in the further research. Ordered domains are seen already over a large scan area of 200 × 200 nm^2. The reconstruction lines of the Au(111)-surface are lifted in the presence of the DNAzyme adlayer due to formation of S-Au bonds, Figure 5A. Zooming in to 100 × 100 nm^2, two kinds of domains become apparent. Domain 1 shows network-like structures, while Domain 2 shows linear arrays (Figure 5B). Smaller bright structures, possibly liberated hemin molecules are also apparent. The fine-structure in Domain 1 resolved to 40 × 40 nm^2 shows both quadratic molecular scale and larger octagonal entities (Figure 5C). The quadratic entities could represent the folded 12G-qs box composed of three vertically stacked planar G-quartets. The octagonal units would then be larger structural entities formed through hydrogen bonds stretching out from the quartets, Figure 5D and further mediated via networks of surface bound water molecules. Similar quartet structures were discovered by the assembly of guanine molecules directly on Au(111) surface in ultra-high vacuum (UHV) as imaged by STM at 350 K.[42] The size of the G-quartet with the four guanine molecules in UHV is 0.67 nm**.** The size of the 12G-qs in aqueous solution presently studied is larger and measured to be 1.6 ± 0.2 nm. The larger side length is most likely caused by water molecules engaged in hydrogen bonding stretching out from the 12G-qs boxes.

Domain 2 is composed of parallel lines (Figure 5B). The origin of these structures is presently more elusive, but the lines could possibly suggest that unfolded single OGN strands are present and could align via hydrogen bonding between the unfolded strands.

View Article Online
DOI: 10.1039/C6FD00091F

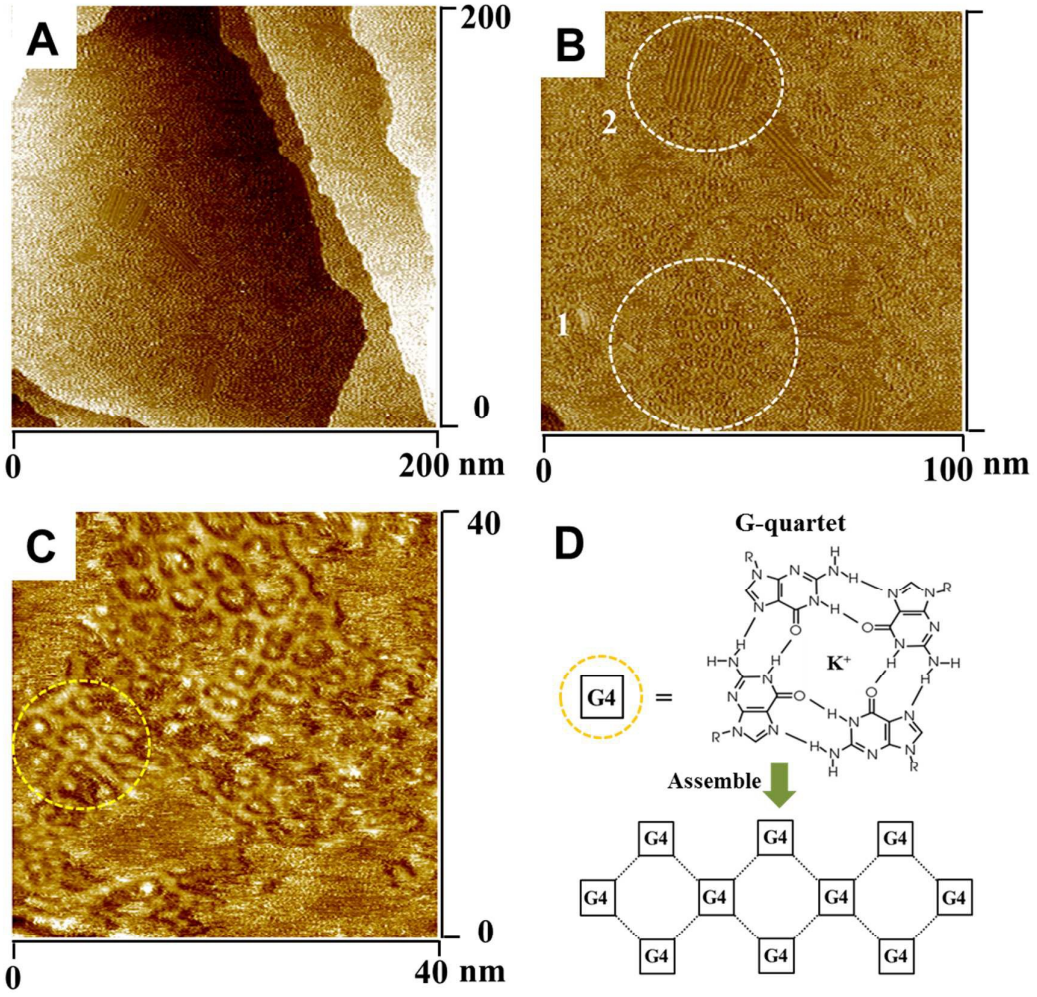

Figure 5. (A−C) *In situ* STM images of DNAzyme adlayer on Au(111)-electrode surface in 5 mM sodium acetate at pH 7.0. E_w = 0.49 V (vs. NHE), V_{bias} = − 0.48 V. I_{tunn} = 0.09 nA. (D) As a comparison, structure of the planar G-quartet and the octagonal superstructure of the G-quadruplex SAMs formed on the Au(111)-electrode surface.

4. Conclusion

Electronic conductivity of redox metalloproteins and metalloenzymes[34,36-39,55,56], and of double strand DNA-based molecules[11-13,16-19,57,58] immobilized at electrochemical interfaces have been explored comprehensively. Electronic conductivity of "non-canonical" DNA forms, quadruplexes in particular have also been addressed, but such reports have only begun to appear much more recently[27-33], and with little if any direct approach to interfacial

View Article Online
DOI: 10.1039/C6FD00091F

electrochemical ET of the quadruplex targets themselves. As noted, perspectives of addressing the electrochemistry of the quadruplexes offer other perspectives: ***(a)*** the box-like qs structure, Figure 1 offers a mechanistic perspective for electronic conductivity through a three-dimensional DNA-based structures more rigid than ds DNA; ***(b)*** The rigid "solid" structure may also hold a perspective for mapping potential induced structural reorientation of the surface immobilized qs DNA adlayers on the atomically planar Au(111)-electrode surfaces similar to what was reported for 20-base ds OGNs bound to spermidine[20] and for other biomolecules such as the amino acid homocysteine[59] and other complex molecules[60] as well as the nucleobases themselves[61]; ***(c)*** surface immobilized G-quadruplexes finally offer perspectives for ultra-sensitive detection of metal ions[40-42], complex biomolecules such as peptides[23-30], and perhaps other analytes.

In the present study we have addressed both the interfacial electrochemical behavior and single-molecule structural *in situ* STM imaging of a DNA quadruplex, viz. the smallest three-quartet stacked 12G-qs immobilized on single-crystal Au(111)-electrode surfaces. The planar macrocyclic Fe(II)/(III) complex hemin terminally bound non-covalently to the quadruplex molecule, or possibly intercalated in the 12G-qs structure is exploited as a redox probe for interfacial electrochemical electron transfer. Biological buffers with pH around 7 were the reaction media.

Hemin itself was found to adsorb directly on the Au(111)-electrode surface and to show complex electrochemistry depending on pH, soaking concentration etc., to be communicated elsewhere. A single monolayer voltammetric redox peak ascribed to the Fe(II)/(III) transition appears, however, at – 0.05 V (NHE) at pH 7. Soaking at hemin concentrations in the sub-μM range gives a coverage of only a few per cent but soaking at high (10 μM) hemin concentration leads to a dense and highly ordered monolayer with a $c(4 \times 3\sqrt{\mathbf{3}})$-2 surface lattice as clearly mapped by *in situ* STM.

12G-qs and the 12G-qs/hemin complex both adsorb on the Au(111)-electrode surface. Voltammetry of hemin-free 12G-qs shows a broad featureless capacitive background but also a conspicuous pair of voltammetric peaks at the significantly negative potentials, – 0.4 to – 0.55 V (vs. NHE). This pair resembles the capacitive peak reported earlier for 20-base pair DNA OGNs with bound spermidine[20]. The triply charged spermidinium cation increases both the structural stability and rigidity of the ds DNA backbone. In this respect the 12G-qs

View Article Online
DOI: 10.1039/C6FD00091F

appears to resemble spermidinium stabilized ds DNA, and we tentatively assign the – 0.4/–0.55 V peaks to potential induced 12G-qs adlayer reorientation. We have not, however, presently reached the same level of support for 12G-qs structural reorganization as for spermidinium bound ds 20-base pair OGNs.

Intriguingly, the hemin voltammetric peak intensity, sharpness, and stability all increase strongly compared with hemin physisorbed directly on the Au(111)-electrode surface, when hemin is bound to 12G-qs on the Au(111)-electrode surface. Close to full monolayer coverage of hemin bound 12G-qs emerges from the CVs, testifying to close to full monolayer coverage of hemin-bound 12G-qs. The well-defined peaks enable estimating the interfacial electrochemical ET rate constant as $6.0 \pm 0.4\ s^{-1}$. This value is high, and as the terminal hemin binding site can be at either end of the 12G-qs target molecule, the standard rate constant can reflect ET of hemin bound either at the adjacent or the remote end of vertically bound or tilted 12G-qs. The electronic charge flow could thus reflect ET through the 12G-qs box, but this conclusion is not presently definite.

A dense monolayer of 12G-qs/hemin complex was supported by *in situ* STM. Domains of G-quartets/octagons ordered collectively possibly via H-bonded water molecules are clearly visible, Figure 5. Formation of ordered adlayers is, however, highly sensitive to preparation conditions, quality of the electrodes, and other controlling factors. Domains of linear structures, suggested to be single-strand unfolded 12G-qs molecules are thus visible together with the quartet structures in the same scan area, Figure 5.

In conclusion, 12G-qs can be immobilized on well-defined Au(111)-electrode surfaces. A capacitive voltammetric peak at negative potentials is indicative of potential induced structural surface reorientation in the adlayer similar to what was reported for spermidine bound 20-base pair ds OGN[20] although not as solidly supported. Hemin bound to surface immobilized 12G-qs's displays well-defined Faradaic voltammetry with much stronger and better defined hemin-based peaks than for hemin directly physisorbed on the Au(111)-surface and with fast interfacial electrochemical electron transfer.

The peak area reflects that a dense monolayer of 12G-qs/hemin DNAzyme has formed, supported by *in situ* STM imaging. Even though still voltammetrically highly active, these attractive looking structures are, however, fragile and at risk of decomposition into both unfolded but still laterally organized 12G single strands and less ordered surface adlayers of

View Article Online
DOI: 10.1039/C6FD00091F

mixed single-entity structures and a disordered background. Work towards optimization of the imaging conditions is in progress. This work will address both tunnelling current/overpotential and current/bias voltage spectroscopy and also target qs structures with two hemin molecules bound. The latter approach would give a clearer view of long-range ET through the 12G-qs structure either by ET directly between the remote hemin group and the electrode surface or by sequential ET that would also involve electron exchange between the two bound hemin molecules.

Acknowledgement

LZ acknowledges the award of a H.C. Ørsted/Marie Curie Co-fund grant. Financial support from The Danish Council for Independent Research for the YDUN project (DFF 4093-00297) and the Lundbeck Foundation for project R141-2013-13273 to JZ is gratefully acknowledged. We wish to thank Professor Jesper Wengel at the Nucleic Acid Center, University of Southern Denmark for providing the thiolated target 12G strand.

References

1. *Electrochemistry of Nucleic Acids and Proteins: Towards Electrochemical Sensors for Genomics and Proteomics*, Eds. E. Paleček, F. Scheller and J. Wang, Elsevier, A Amsterdam, 2005.
2. A. Sassolas, B.D. Leca-Bouvier and J.L. Blum, Chem. Rev. 2008, **108**, 109-139.
3. Chapters in: *DNA Conjugates and Sensors*, Ed. K.R. Fox and T. Brown, RSC Publishing, London, 2012.
4. *Electrochemical DNA Biosensors*, Ed. M.S. Ozsoz, Pan Stanford Publishing, Singapore, 2012.
5. H.B. Gray and J.R. Winkler, Proc. Nat. Acad. Sci. USA, 2005, **102**, 3534-3539.
6. J.J. Warren, M.E. Ener, A. Vlček, Jr., J.R. Winkler and H.B Gray, Coord. Chem. Rev., 2012, **256**, 2478-2487.
7. C.C. Moser, J.L.R. Anderson and P.L. Dutton, Biochim. Biophys. Acta, 2010, **1797**, 1573-1586.
8. J.R. Winkler, A.R. Dunn, C.R. Hess and H.B. Gray, in *Bioinorganic Electrochemistry*, Eds. O. Hammerich and J. Ulstrup, Springer, Dordrecht, 2008, pp.1-23.

View Article Online
DOI: 10.1039/C6FD00091F

9. A.M. Kuznetsov and J. Ulstrup, in *Bioinorganic Electrochemistry*, Eds. O. Hammerich and J. Ulstrup, Springer, Dordrecht, 2008, pp.161-205.
10. N.J. Turro and J.K. Barton, J. Biol. Inorg. Chem., 1998, **3**, 201-209.
11. M.A. O'Neil and J.K Barton, in*: Charge Transfer in DNA: From Mechanism to A Application*, Ed. H.-A. Wagenknecht, Wiley-VCH, Weinheim, 2004, pp. 27-75.
12. J.C. Genereux and J.K. Barton, Chem. Rev., 2010, 110, 1642-1661.
13. E.L.S. Wong, E. Chow and J. Gooding, Langmuir, 2005, **21**, 6957-6965.
14. J. Jortner. M. Bixon, T. Langenbacher and M.E. Michel-Beyerle, Proc. Nat. Acad. Sci. USA, 1998, **95**, 12759-12765.
15. M- Bixon, B. Giese, S. Wessely, T. Langenbacher, M.E. Michel-Beyerle and J. Jortner, Proc. Nat. Acad. Sci. USA, 1999, **96**, 11713-11716.
16. Chapters in: *Charge Transfer in DNA: From Mechanism to Application*, Ed. H.-A. Wagenknecht, Wiley-VCH, Weinheim, 2004.
17. M.G. Hill and S.O. Kelley, in *Bioinorganic Electrochemistry*, Eds. O. Hammerich and J. Ulstrup, Springer, Dordrecht, 2008, pp.129-160.
18. C.G. Pheenwy and J.K. Barton, Langmuir, 2012, **28**, 7063-7070, and references there.
19. N.B. Muren, E.D. Olmon and J.K.Barton, PhysChemChemPhys. 2012, **14**, 13754-13771.
20. P. Salvatore, K.K. Karlsen, A.G. Hansen, J. Zhang, R.J. Nichols and J. Ulstrup, J. Am. Chem. Soc., 2012, **134**, 19092-19098.
21. A.A. Kornyshev and S. Leikin,, Phys. Rev. Lett. 2001, **86**, 3666-3669.
22. A.A. Kornyshev, D.J. Lee, S. Leikin and A. Wynveen, Rev. Mod. Phys., 2007, **79**, 943-996.
23. S. Müller, S. Kumari, R. Rodriguez and S. Balasubramanian, Nat. Chem., 2010, **2**, 1095-1098.
24. A.N. Lane, J.B. Chaires, R.D. Gray and J.O. Trent, Nucleic Acids Res., 2008, **36**, 5482-5515.
25. D. Koirala, S. Dhakal, B. Ashbridge, Y. Sannohe, R. Rodriguez, H. Sugiyama, S. Balasubramanian and H. Mao, Nat. Chem., 2011, **3**, 782-787.
26. T. Li, L. Shi, E. Wang and S. Dong, Chem. Eur. J., 2009, **15**, 1036-1042.
27. B. Ruttkay-Nedecky, J. Kudr, L. Nejdi, D. Maskova, R. Kizek and V. Adam, Molecules, 2013, **18**, 14760-14779.

View Article Online
DOI: 10.1039/C6FD00091F

28. O. Doluca, J.M. Withers and V.V. Filichev, Chem. Rev. 2013, **113**, 3044-3083.

29. S. Liu, S.H. Weisbrod, Z. Tang, A. Marx, E. Scheer and A. Erbe, Angew. Chem. Int. Ed., 2010, **49**, 3313-3316.

30. S- Liu, X- Zhang, W. Luo, Z. Wang, X. Guo, M.L. Sterigerwald and X. Fang, Angew. Chem. Int. Ed., 2010, **50**, 2496-2502.

31. J. Choi, J. Park, A. Tanaka, M.J. Park, Y.J. Jang, M. Fujitsuka, S.K. Kim and T. Majima, Angew. Chem. Int. Ed., 2013, **52**, 1134-1138.

32. C.J. Lech, A.T. Phan, M.E. Michel-Beyerle and A.A. Voityuk, J. Phys. Chem., 2013, **117**, 9851-9856.

33. A. de Rache, T. Doneux and C. Buess-Hermann, Anal. Chem., 2014, **86**, 8057-8065.

34. J. Zhang, Q. Chi, A.G. Hansen, P. S. Jensen, P. Salvatore and J. Ulstrup, FEBS Letters, 2012, **586**, 526-535.

35. A.G. Hansen, P. Salvatore, K.K. Karlsen, R.J. Nichols, J. Wengel and J. Ulstrup, PhysChemChem Phys, 2013, **15**, 776-786.

36. J. Zhang, A.M. Kuznetsov, I.G. Medvedev, Q. Chi, T. Albrecht, P.S. Jensen and J. Ulstrup, Chem. Rev., 2008, **108**, 2737-2791.

37. E.A. Della Pia, Q. Chi, J.E. Macdonald, J. Ulstrup, D.D. Jones and M. Elliott, Nanoscale, 2012, **4**, 7106-7113.

38. B. Bonanni, L. Andolfi, A.R. Bizarri and S. Cannistraro, J. Phys. Chem. B, 2007, **111**, 5062-5075.

39. J.M. Artés, Y. Li, J. Qi, M.P. Anantram and J. Hihath, Nat. Comm., 2015, DOI:10.1038/ncomms9870.

40. T. Li, E. Wang, S. Dong, J. Am. Chem. Soc., 2009, **131**, 15082-15083.

41. G. Pelossof, R. Tel-Vered and I. Willner, Anal. Chem., 2012, **84**, 3703-3709.

42. 40. C. Zhang, L. Xie, L. Wang, H. Kong, Q. Tan and W. Xu, J. Am. Chem. Soc., 2015, **137**, 11795-11800.

43. A. Hamelin, J. Electroanal. Chem., 1996, **407**, 1-11.

44. Q. Chi, J. Zhang, E.P. Friis, J. E.T. Andersen and J. Ulstrup, Electrochem. Comm., 1999, **1,** 91- 96.

45. Q. Chi, J. Zhang, J.U. Nielsen, E.P. Friis, I. Chorkendorff, G.W. Canters, J.E.T. Andersen and J. Ulstrup, J. Am. Chem. Soc., 2000, **122**, 4047-4055.

View Article Online
DOI: 10.1039/C6FD00091F

46. J. Zhang, A. Bilič, J.R. Reimers, N.S. Hush and J. Ulstrup, J. Phys. Chem. B, 2005, **109**, 15355- 15367.

47. J. Zhang, Q. Chi, J.E.T. Andersen, E.P. Friis and J.U. Nielsen, J. Ulstrup, Langmuir, 2000, **16**, 7229-7237.

48. N.J. Tao, G. Cardenas, F. Cunha and Z. Shi, Langmuir, 11 (1995) 4445-4448.

49 S. Yoshimoto, A. Tada and K. Itaya, J. Phys. Chem. B, 108 (2004) 5171-5174.

50. S. Yoshimoto, N. Yokoo, T. Fukuda, N. Kobayashi and K. Itaya, Chem. Comm., (2006) 500- 502.

51. J.R. Reimers, D. Panduwinata, J. Visser, Y. Chin. C. Tang, L., Goerick, M.J. Ford, M. Sintic T.-J. Sum, M.J.J. Coenen, B.L.M. Henriksen, J.A.A.W. Elemens, N.S. Hush and M.J. Crossley, Proc. Nat. Acad. Sci. USA, 2015, **112**, E6101-E6110.

52. S. Yoshimoto, A. Tada, K. Suto and K. Itaya, J. Phys. Chem. B 2003, **107**, 5836-5843.

53. S. Yoshimoto, A. Tada, and K. Itaya, J. Phys. Chem. B 2004, **108**, 5171-5174.

54. J. Zhang, A.C. Welinder, Q. Chi and J. Ulstrup, PhysChemChemPhys, 2011, **13**, 5526-5545.

55. J. Zhang, A.C. Welinder, A.G. Hansen, H.E.M. Christensen and J. Ulstrup, J. Phys. Chem. B, 2003, **104**, 12480-12484.

56. V. Climent, J. Zhang, E.P. Friis, L.H. Østergaard and J. Ulstrup, J. Phys. Chem. C, 2012, **116**, 1232-1243.

57. T. Oshiro and M. Maeda, Chem. Comm., 2010, **46**, 2581-2583.

58. T. Nishino and P.T. Bui, Chem. Comm., 2013, **49**, 3437-3439.

59. J. Zhang, A. Demetriou, A.C. Welinder, T. Albrecht, R.J. Nichols and J. Ulstrup, Chem. Phys., 2005, **319**, 210-221.

60. G.J. Su, H.M. Zhang, L.J. Wan, C.L. Bai and T. Wandlowski, J. Phys. Chem. B, 2004, **108**, 1931-1937.

61. M.H. Holzle, T. Wandlowski and D.M., Kolb, J. Electroanal. Chem., 1995, **394**, 271-275.